JAAS

PAPER

Cite this: *J. Anal. At. Spectrom.*, 2019, **34**, 874

Three dimensional secondary ion mass spectrometry imaging (3D-SIMS) of *Aedes aegypti* ovarian follicles†

Anthony Castellanos,[a] Cesar E. Ramirez,[a] Veronika Michalkova,[b] Marcela Nouzova,[bc] Fernando G. Noriega[bd] and Francisco Fernández-Lima *[ad]

Received 1st December 2018
Accepted 21st February 2019

DOI: 10.1039/c8ja00425k

rsc.li/jaas

The mobilization of nutrient reserves into the ovaries of *Aedes aegypti* mosquitoes after sugar-feeding plays a vital role in the female's reproductive maturation. In the present work, three-dimensional secondary ion mass spectrometry imaging (3D-SIMS) was used to generate ultrahigh spatial resolution (~1 μm) chemical maps and study the composition and spatial distribution of lipids at the single ovarian follicle level (~100 μm in size). 3D-Mass Spectrometry Imaging (3D-MSI) allowed the identification of cellular types in the follicle (oocyte, nurse and follicular cells) using endogenous markers, and revealed that most of the triacyglycerides (TGs) were compartmentalized in the oocyte region. By comparing follicles from water-fed and sugar-fed females ($n = 2$), 3D-MSI-Time of Flight-SIMS showed that TGs were more abundant in ovarian follicles of sugar-fed females; despite relative sample reproducibility per feeding condition, more biological replicates will better support the trends observed. While the current 3D-MSI-TOF-SIMS does not permit MS/MS analysis of the lipid species, complementary LC-MS/MS analysis of the ovarian follicles aided tentative lipid assignments of the SIMS data. The combination of these MS approaches is giving us a first glimpse of the distribution of functionally relevant ovarian lipid molecules at the cellular level. These new tools can be used to investigate the roles of different lipids on follicle fitness and overall mosquito reproductive output.

Introduction

Mass spectrometry-based techniques are the analytical gold standard for the separation, identification, and quantification of lipids in biological samples.[1,2] Typically, total lipid analysis by MS is based on extraction protocols from biological matrices followed by liquid chromatography coupled to tandem mass spectrometry (*e.g.*, LC-MS/MS).[3,4] However, depending on the biological question, the chemical mapping of the lipid distribution in biological systems using mass spectrometry imaging (MSI) techniques is mandatory. For example, liquid based junctions, jets and micro-junctions (*i.e.*, liquid extraction surface analysis, or LESA),[5,6] desorption electrospray ionization (DESI),[7,8] and nanospray desorption electrospray ionization (nano-DESI)[9] can provide lipid chemical maps with spatial resolution down to ~600 μm, ~50 μm,[10,11] and ~10 μm,[12] respectively, under ambient conditions and without the need of any surface treatment. Other MSI techniques using laser sources can provide a higher spatial resolution (10–50 μm or down to few μm using special arrangements[13]) at ambient or vacuum conditions, but typically require the coating of the biological surfaces with a matrix (*i.e.*, MALDI[14–16]); the matrix choice and application method determine the selectivity of analytes and the crystal size can become the limiting factor of the spatial resolution.[16,17] For MSI lipid analysis with high spatial resolution (<1 μm),[18–21] ion beams are typically used under vacuum conditions[22] without the need of surface treatment (*i.e.*, secondary ion mass spectrometry, SIMS);[23] SIMS spatial resolution and secondary ion yield varies with the projectile size (*e.g.*, from atomic to poly-atomic to cluster beams) and incident energy.[24–33]

Lipid MSI has been mainly performed by 2D imaging of subsequent sample sections, with consequent loss of 3D information due to the thickness of each slide (typically tens of μm). Alternatively, with the advent of "soft" ion probes (*e.g.*, fullerenes,[34–36] argon clusters,[37,38] water clusters,[39] and carbon dioxide clusters[40]), MSI can interrogate biological surfaces "layer by layer" (nanometer depth resolution) with ultrahigh spatial resolution using SIMS.[41] In particular, 2D and 3D SIMS

[a]*Department of Chemistry and Biochemistry, Florida International University, 11200 SW 8th St AHC4-233, Miami, FL 33199, USA. E-mail: fernandf@fiu.edu*
[b]*Department of Biological Sciences, Florida International University, Miami, Florida, 33199, USA*
[c]*Institute of Parasitology, Biology Centre CAS, Ceske, Budejovice, Czech Republic*
[d]*Biomolecular Sciences Institute, Florida International University, Miami, Florida, 33199, USA*

† Electronic supplementary information (ESI) available. See DOI: 10.1039/c8ja00425k

are exceptionally suited for the lipid study of small and complex biological samples such as insects at the single cell level.[42–45]

Lipids are extremely important for the development and reproduction of *Ae. aegypti* mosquitoes. The nutritional and hormonal regulation of reproduction is a critical component of mosquito female fitness, and therefore of the ability to transmit diseases.[46–48] Mosquito-borne diseases such as Zika, Dengue, Chikungunya and Malaria constitute critical threats to public health in many parts of the world.[49–52] Each of the two ovaries of the female of *Ae. aegypti* mosquitoes contains about 60 ovarioles with germaria attached to primary and secondary follicles. Each follicle consists of one oocyte plus 7 nurse cells that are surrounded by follicular epithelial cells.[53] There are three periods in the development of the primary ovarian follicles during a gonotrophic cycle: previtellogenesis (PVG), ovarian resting stage (ORS) and vitellogenesis (VG). Females emerge with immature primary follicles that grow into mature PVG follicles in the next 48–72 h; oocytes remain in a dynamic "state of arrest", and will enter VG only after a blood meal.[54] *Ae. aegypti* females can lay over 120 eggs in a gonotrophic cycle; therefore, a tightly regulated control of nutrient allocations to the ovaries is critical for survival.[55,56] The ovarian resting stage in *Ae. aegypti* is a period marked by constant adjustment of the reproductive output based on nutritional status; this adjustment occurs mostly through follicular resorption by apoptosis.[55]

During their PVG maturation, mosquito oocytes increase their lipid content several-fold.[57] The main source of lipids for oocytes comes from larval accrual (teneral) reserves, as well as from sugar meals taken by the adult.[58] Female mosquitoes are subject to 'trade-offs' between the energetic demands of reproduction and the energy required to survive; they must consider the effects of immediate resource allocations on future reproduction and overall fitness.[55,56] While previous studies have described that high sugar diets prompt accumulation of lipids in the oocyte,[56] little is known about the lipid identities, composition and distribution within a single follicle.

In the current study, for the first time, 3D-SIMS is utilized for the analysis of lipid composition and lipid spatial distribution of single follicles from ovaries of *Ae. aegypti* mosquitoes. An organism model that recreates different ovarian phenotypes during the ORS based on a sugar diet is utilized to evaluate the reproductive output and lipid content at the follicle level. Results demonstrated the capability of 3D-SIMS to generate chemical maps with high spatial resolution and the visualization of intact lipids. In particular, we demonstrated that sugar-feeding results in increased levels of polyunsaturated triacylglycerides (TG) with long chain fatty acids, such as TG 48:1, 48:2, 50:1 and 50:2; with most of the TGs compartmentalized in the oocyte region.

Materials and methods

Mosquito samples

Ae. aegypti of the Rockefeller strain were raised at 28 °C with 80% humidity, at a 16 hour light and 8 hour dark cycle.[55] After adult eclosion, females were fed from either a cotton pad soaked in a 20% sucrose solution or a water-soaked cotton pad (0% sucrose). On the fifth day, females were collected and cold anaesthetized over ice. Ovaries were dissected in phosphate-buffered saline (PBS), stained with a DAPI solution (prepared 3 μM in PBS), and rinsed in a solution of 150 mM ammonium acetate adjusted to a pH of 7.4.

LC-MS/MS analysis

Ten mosquito ovaries were dissected and transferred into a 1.5 mL Eppendorf tube containing 100 μL of 50 : 50 1-butanol/methanol. A 2.5 μL aliquot of a 1 mM solution of the antioxidant butylated hydroxytoluene (BHT) was added to prevent lipid degradation. A mix of several deuterated lipids (10 μL of Splash Lipidomix, Avanti Polar Lipids, Alabaster, AL) was introduced for internal standardization. Kontes polypropylene pellet pestles (Fisher Scientific, Pittsburgh, PA) were used with a cordless motor to mechanically homogenize ovaries for 10 seconds. The pestle was then rinsed with 200 μL of 1-butanol/methanol. Samples were sonicated for 30 minutes at room temperature, and centrifuged at 1600 × *g* for 10 minutes. The supernatants were then transferred into 2 mL autosampler silanized vials (Thermo Fisher Scientific, Waltham, MA).

LC-MS/MS analyses were performed on a Prominence LC-20 CE Ultra-Fast Liquid Chromatograph (Shimadzu, Kyoto, Japan) equipped with a Dionex Acclaim C18 Column (250 × 2.1 mm, 5 μm) (Thermo Scientific, Sunnyvale, CA), performing gradient separations between 40 : 60 ACN : water and 89 : 10 : 1 solution of isopropyl alcohol (IPA) : ACN : water (both with 10 mM (NH_4COOH) and 0.1% FA).

Detection was performed by a Bruker timsTOF quadrupole-time of flight (QTOF) mass spectrometer (Billerica, MA) equipped with an electrospray ionization source. The instrument was operated under data-dependent scan acquisition mode, performing MS/MS *via* collision induced dissociation (CID). Lipid candidate assignments were made using Metaboscape (Bruker Daltonics Inc.) and SimLipid (PREMIER Biosoft, Palo Alto, CA). MS/MS assignments were manually curated and a 10 ppm tolerance was used for MS^1.

Follicle freeze-drying procedure

Follicles were prepared using a freeze-drying method,[18] optimized here for fluorescence imaging and 3D-TOF-SIMS analysis. Ovaries were first placed in a 150 mM ammonium acetate droplet on an ITO coated glass slide, and individual follicles were mechanically separated using microdissection pins. The droplet containing ovarian follicles was sandwiched with a second ITO slide, using glass coverslips as a spacer (~20 μm) on either end. The assembly was held in place using binder clips, and subsequently immersed in liquid nitrogen for several minutes. The binder clips were then removed, and the ITO slides were separated while still immersed in liquid nitrogen, akin to freeze-fracture techniques.[59] The sample slides were then transferred into a custom-built vacuum dryer and allowed to dry as liquid nitrogen boiled off and returned to room temperature. The sandwich technique employed here allowed

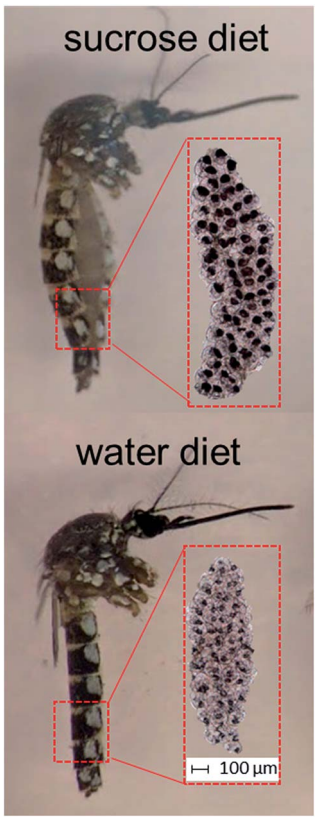

Fig. 1 Optical images of 5 day old adult *Ae. aegypti*. The ovaries of the sucrose-fed female are larger than the water-fed counterpart.

for follicles to remain relatively flat and attached to the slide, enabling subsequent microscopy. Afterwards, ITO slides were mounted on an ION-TOF top mount stage for TOF-SIMS analysis. The use of ammonium salts for washing and freeze-drying have been previously utilized to prevent the accumulation of non-volatile salts such as sodium and potassium, commonly present in buffer solutions.[60] In addition, freeze-drying preserves cell morphology without the use of chemical fixatives or alcohol dehydration, which could cause a displacement of diffusible ions and membrane phospholipids.[61,62]

Microscopy

Following the freeze-drying of ovarian follicles, sample slides were inspected with a Nikon Eclipse Ts2R-FL inverted microscope (Nikon Instruments Inc., Melville, NY). Phase contrast images were recorded with a ×20 objective using a 30 ms exposure time. A Nikon DAPI filter was used to visualize stained ovarian follicles at an exposure time of 600 ms. Observations of freeze-dried samples revealed that our sample preparations yielded relatively flat individual follicles, with most fluorescent nurse cells in focus and minimal instances of fractures.

3D-TOF-SIMS analysis

A TOF-SIMS 5 instrument retrofitted with a 25 kV Bismuth liquid metal ion gun and a 20 kV argon cluster sputtering (ION-TOF GmbH, Münster, Germany) was used. The 3D-TOF-SIMS spectra were collected in High Current Bunched mode (HCBU). 2D-MSI analyses were performed by rastering a Bi_3^+ primary ion beam over a 200 × 200 µm^2 area centered on the ovarian follicles. Total 2D-MSI primary ion doses were ~1 × 10^{12} ions per cm^2 per sputter cycle, with a measured spatial resolution of <3 µm. The 20 keV argon cluster ion beam (Ar_{2200}^+) was used to sputter the sample surface at an ion dose of ~1 × 10^{13} ions per cm^2 in between 2D-MSI scans. That is, the 3D-MSI data consisted of non-interlaced cycles of Bi_3^+ and Ar_{2200}^+ ion bombardment. After the samples substrate was reached during the 3D analysis, the summed signals from all 3D voxels were used for 2D visualization and quantification. 3D-TOF-SIMS analyses were carried out in duplicate on follicles from either diet. Ion beam-induced charge accumulation on the sample surface was compensated with an electron flooding gun (21 eV). Secondary ions were accelerated to a kinetic energy of 3 KeV toward a field-free region and a single-stage reflectron. Secondary ions were post-accelerated to a kinetic energy of 10 KeV, before reaching a hybrid detector, composed of a multi-channel plate scintillator, and a photomultiplier detection system. In the positive polarity, mass spectra were internally calibrated using the commonly observed hydrocarbon series: C^+, CH^+, CH_2^+, CH_3^+, $C_2H_3^+$, and $C_2H_5^+$, as well as the commonly observed lipid fragment ions $C_5H_{14}NO^+$ and $C_5H_{15}NPO_4^+$.[30] A

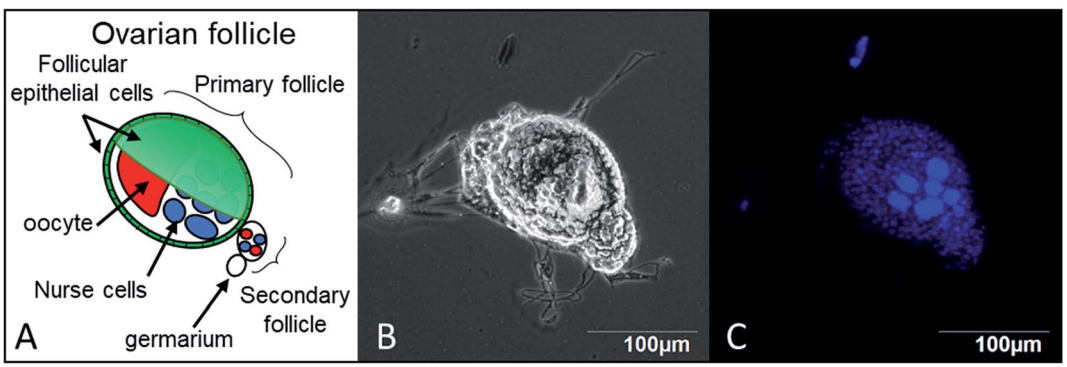

Fig. 2 (A) Schematic, (B) optical, and (C) fluorescence images of a previtellogenic ovarian follicle of *Ae. aegypti*. Each follicle consists of one oocyte plus 7 nurse cells that are surrounded by follicular epithelial cells. A secondary follicle and the germarium are also visualized distal to the oocyte.

mass resolution of $R = 3000$ at 851 m/z (TG 50:3 $[M + Na]^+$ ion) was observed during the positive mode HCBU analysis. TOF-SIMS signals were labeled based on LC-MS/MS analysis from replicate samples with a mass tolerance of 10 ppm in MS^1 and with MS/MS information. A TOF-SIMS mass accuracy of <100 ppm, attributed to the non-flat nature of the sample, was observed for all annotated PC and TG.

Data were collected and processed using the ION-TOF SurfaceLab 6 V6.4 (Münster, Germany). The NESAC/BIO's NBToolbox V2.7 software (available at http://mvsa.nb.uw.edu) was used

Table 1 Tentative assignments of signals observed in 3D-TOF-SIMS analysis of *Ae. aegypti* ovarian follicles. LC-MS/MS assignments were manually curated and a 10 ppm tolerance was used for the parent ion database search

TOF SIMS m/z	Tentative assignment	Proposed chemical formula	Theoretical m/z	LC-MS/MS
730.5	PC 32:2 (16:1/16:1) $[M + H]^+$	$C_{40}H_{77}NO_8P$	730.5381	HG-H_2O 166.066, HG 184.0801, M-16:1-H_2O 476.3152, M-NL 547.4637, M-$C_5H_{13}NO_3P$-H_2O 547.4637
732.4	PC 32:1 (16:0/16:1) $[M + H]^+$	$C_{40}H_{79}NO_8P$	732.5538	$C_5H_{13}N$ 86.1116, M-$C_{35}H_{65}O_7P$-H_2O 86.1116, HG-H_2O 166.0694, HG 184.0799, M-16:0-H_2O 476.3183, M-16:1-H_2O 478.3238
734.4	PC 32:0 (16:0/16:0) $[M + H]^+$	$C_{40}H_{81}NO_8P$	734.5694	M-16:0-H_2O 478.2291, M-C_2H_6N 691.4202, M 734.463
756.5	PC 34:3 (16:1/18:2) $[M + H]^+$	$C_{42}H_{79}NO_8P$	756.5538	HG-H_2O 166.0788, HG 184.0801, 15:1 C=O$^+$ 237.2243, M-18:2-H_2O 476.3126, M-16:1-H_2O 502.3297, M-16:1520.3345
758.4	PC 34:2 $[M + H]^+$	$C_{42}H_{81}NO_8P$	758.5694	HG-H_2O 166.0686, HG 184.0787
760.4	PC 34:1 (16:0/18:1) $[M + H]^+$	$C_{42}H_{83}NO_8P$	760.5851	HG-H_2O 166.0704, HG 184.0799, M-18:1-H_2O 478.3262, M-18:1496.3315, M-16:0-H_2O 504.3437
786.4	PC 36:2 (18:1/18:1) $[M + H]^+$	$C_{44}H_{85}NO_8P$	786.6007	HG-H_2O 166.0671, HG 184.0796, 17:1 C=O$^+$ 265.2517, M-18:1-H_2O 504.3393, M-18:1522.359, M-NL 603.544, M-$C_5H_{13}NO_3P$-H_2O 603.544
823.6	TG 48:3 (16:1/16:1/16:1) $[M + Na]^+$	$C_{51}H_{92}O_6Na$	823.6786	M-16:1569.4508
	TG 48:3 (14:1/16:1/18:1) $[M + Na]^+$	$C_{51}H_{92}O_6Na$	823.6786	15:1 C=O$^+$ 237.2207, M-18:1519.4371, M-18:1541.4167, M-16:1547.4674, M-14:1575.4999, M 823.6528
825.6	TG 48:2 (16:0/16:1/16:1) $[M + Na]^+$	$C_{51}H_{94}O_6Na$	825.6943	15:1 C=O$^+$ 237.2268, 15:0 C=O$^+$ 239.2386, M-16:0547.4672, M-16:1549.482, M-16:0569.4498, M-16:1571.4654, M 825.6911
827.6	TG 48:1 (16:0/16:0/16:1) $[M + Na]^+$	$C_{51}H_{96}O_6Na$	827.7099	15:1 C=O$^+$ 237.225, 15:0 C=O$^+$ 239.242, M-16:0549.4849, M-16:1551.4965, M-16:0571.4674, M-16:1573.4857
849.6	TG 50:4 $[M + Na]^+$	$C_{53}H_{94}O_6Na$	849.6943	
851.6	TG 50:3 (16:1/16:1/18:1) $[M + Na]^+$	$C_{53}H_{96}O_6Na$	851.7099	15:1 C=O$^+$ 237.2233, M-18:1547.4704, M-16:1575.5006, M-16:1597.4813
853.6	TG 50:2 $[M + Na]^+$	$C_{53}H_{98}O_6Na$	853.7256	
855.6	TG 50:1 (16:0/16:1/18:0) $[M + Na]^+$	$C_{53}H_{100}O_6Na$	855.7412	M-18:0549.4957, M-16:1579.5271
	TG 50:1 (16:0/16:0/18:1) $[M + Na]^+$	$C_{53}H_{100}O_6Na$	855.7412	15:0 C=O$^+$ 239.2402, 17:1 C=O$^+$ 265.2562, M-18:1551.4988, M-18:1573.4829, M-16:0577.5165, M-16:0599.4967, M 855.7492
877.6	TG 52:4 $[M + Na]^+$	$C_{55}H_{98}O_6Na$	877.7256	
879.6	TG 52:3 $[M + Na]^+$	$C_{55}H_{100}O_6Na$	879.7436	15:1 C=O$^+$ 237.2205, 17:1 C=O$^+$ 265.2538, M-20:4575.5001, M-18:1597.4808, M-16:1625.5152, M 879.7376
881.7	TG 52:2 (16:1/18:0/18:1) $[M + Na]^+$	$C_{55}H_{102}O_6Na$	881.7569	15:1 C=O$^+$ 237.2273, 17:1 C=O$^+$ 265.2519, 17:0 C=O$^+$ 267.2516, M-18:0575.4972, M-18:1577.5128, M-18:0597.4911, M-18:1599.5001, M-16:1605.5454, M-16:1627.5321, M 881.7615
883.7	TG 52:1 (16:0/16:1/20:0) $[M + Na]^+$	$C_{55}H1_{04}O_6Na$	883.7725	15:1 C=O$^+$ 237.2269, 15:0 C=O$^+$ 239.2438, M-20:0549.4856, M-20:0571.4671, M-16:0605.5491, M-16:1607.5609, M-16:0627.5306, M-16:1629.5331, M 883.7721
905.7	TG 54:4 $[M + Na]^+$	$C_{57}H_{102}O_6Na$	905.7569	
907.7	TG 54:3 $[M + Na]^+$	$C_{57}H_{104}O_6Na$	907.7725	
909.7	TG 54:2 $[M + Na]^+$	$C_{57}H_{106}O_6Na$	909.7882	

to correct the z-axis and reconstruct depth profile data assuming a constant sputter rate.

Secondary ion yields (Y_{SI}) were calculated by normalizing the secondary ion intensity to the fluence of the primary ion beam and to the size of the region of interest (ROI) for direct comparison between 3D-MSI scans of the sample composition.[18] That is, fluctuations in the primary ion beam and the total 3D interrogated surface area are accounted for and the resulting units for Y_{SI} are the number of secondary ions detected per primary ion impact.

$$Y_{\mathrm{SIfollicle}} = \frac{\sum \text{secondary ions}}{\sum \text{ROI follicle } (\mathrm{cm}^2) \times \text{fluence } (\text{primary ions per } \mathrm{cm}^2)} \quad (1)$$

Results and discussion

A fundamental aspect of animal life history is the ability of an organism to convert available resources into usable nutrients and energy for maintenance, activity and reproduction. Lipids are the major form of energy storage in animals, and in insects, lipids imported from circulation provide most of the energy and nutrients required during egg development.[63] In the mosquito *Culex quinquefasciatus*, ~90% of the energy used during embryogenesis originates from lipids.[64] In *Ae. aegypti*, ~80% of lipids found in eggs are derived from regular sugar meals before blood feeding.[46,65] To better understand the roles of sugar-feeding derived lipid reserves on mosquito ovarian development, we compared ovarian follicles from water-fed and sugar-fed *Ae. aegypti* females, a mosquito experimental model previously developed to study the effect of nutrition on mosquito reproduction.[55,56] Females were isolated at adult eclosion, and raised for 5 days on either a 20% sucrose solution or water. Ovaries from sugar-fed females were larger than those from water-fed females, with the oocytes clearly visible with light microscopy (Fig. 1).

Our first challenge was to optimize a sample preparation protocol that preserves the structural features of the follicle without interfering with the SIMS analysis. To this end, DAPI staining served as a quality control following the freeze-drying procedure discussed in the Methods section. Fig. 2 provides a phase contrast and fluorescence image of an ovarian follicle after freeze-drying. As the follicle scheme illustrates, a suitable protocol should allow the visualization of several nurse cells surrounded by the follicular epithelium; with the oocyte in a distal position in reference to the secondary follicle and the germarium (Fig. 2).

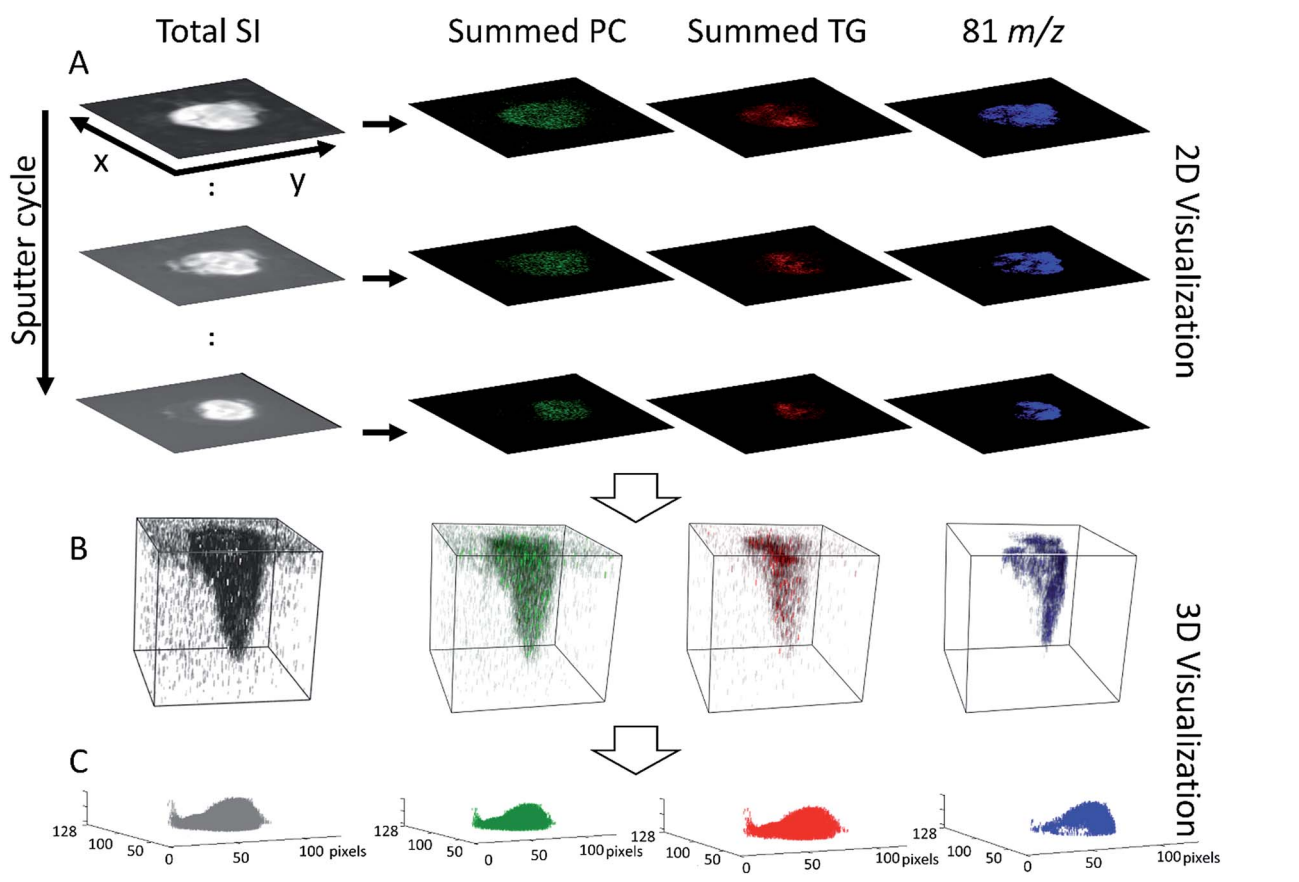

Fig. 3 Visualization of the 3D-MSI analysis of freeze-dried ovarian follicle from a sucrose-diet insect using dual beam TOF-SIMS. (A) 2D slices showing phosphatidylcholine (PC), triacylglyceride (TG) and ribose (81 m/z), (B) 3D-MSI composite, and (C) software corrected 3D reconstruction of non-flat surfaces. The 2D representations correspond to a field of view of 200 × 200 μm. In (C), the x and y axis are shown in pixels (1 pixel = 1.56 μm).

Assignment of lipid species

After verifying the structural integrity of all samples, follicles from both feeding conditions were subjected to 3D-TOF-SIMS analysis. While the TOF-SIMS platform offers reasonable mass resolution (*e.g.*, <10 000), the complexity of biological samples makes it insufficient for unambiguous chemical formula assignment.[66] Our current 3D-MSI platform does not allow for MS/MS analysis; therefore, replicate samples were analyzed by LC-MS/MS to confirm the identification of lipid species. A comprehensive list of the 3D-TOF-SIMS assignments and the supporting MS^2 information can be found in Table 1. Pseudo-molecular secondary ions for phosphatidylcholines (PC) of the form $[M + H]^+$ and triglycerides (TG) of the form $[M + Na]^+$ were primarily observed during 3D-TOF SIMS positive ion mode. Lipid species are abbreviated herein according to lipid class and the number of carbons and double bonds along fatty acyl tails is provided. For example, TG (16:1/16:1/16:1) refers to a triacylglyceride with three fatty acyl groups, each with a 16 carbon chain containing only one double bond.

3D mapping of lipid species

In Fig. 3, the summed 3D signals of several PCs and TGs are depicted in green and red, respectively for follicles from sucrose-diet females. The 3D-TOF-SIMS has a major advantage compared to other 3D-MSI techniques, enabling full access to the 3D information.[18,67] This capability is illustrated in Fig. 3, where successive 2D-MSI heat maps are generated with the Bi_3^+ analytical beam between Ar_{2200}^+ sputtering cycles are visualized. A comprehensive molecular description of species within the follicle is only possible using the 3D-MSI analysis due to the heterogeneity and morphology of the mosquito follicles. Significant advantage when compared to other 3D tools (*e.g.*, confocal microscopy) is that 3D-MSI TOF MS allows for the simultaneous detection of multiple *m*/*z* signal. After the samples substrate was reached during the 3D analysis, the summed signals from all 3D voxels were used for 2D visualization and quantification. However, caution should be taken when constructing such 3D-MSIs since sputtering rates depend on the sample composition. For the analysis presented, a *z*-axis correction relative to the flat substrate was used for a reconstructed visualization of the mosquito follicles (see more details of 3D reconstruction of non-flat samples in ref. 68). ESI Fig. S1† depicts aerial three-dimensional visualization of selected *m*/*z* ions.

The *m*/*z* of 81.03 was tentatively assigned as $C_5H_5O^+$, a fragment ion of ribose previously reported in SIMS analyses of DNA and ribose standards as well as in mammalian cells.[69–71] This *m*/*z* of 81.03 ion (blue) was co-located with DAPI-stained nurse cells. Nurse cells synthesize large amounts of RNA, which is transferred to the developing oocyte.

Sum signal of the 3D-MSI analysis were used to build a complementary 2D representation (top view) of the follicle PCs (green), TGs (red) and ribose (*m*/*z* 81.03, blue) signals in Fig. 4. When compared to the diagram of the follicle in Fig. 1, these species were demonstrated to localize to the follicular epithelium, oocyte, and nurse cells, respectively. Readers are referred to Table 1 for a comprehensive list of the *m*/*z* and their corresponding assignments for PC and TG. Note that different from other imaging techniques where labeling is required, the *m*/*z* channels used to reconstruct the follicle structure are endogenous to the sample. This feature makes 3D-TOF-SIMS a powerful label-free technique for the analysis of biologically relevant molecules.

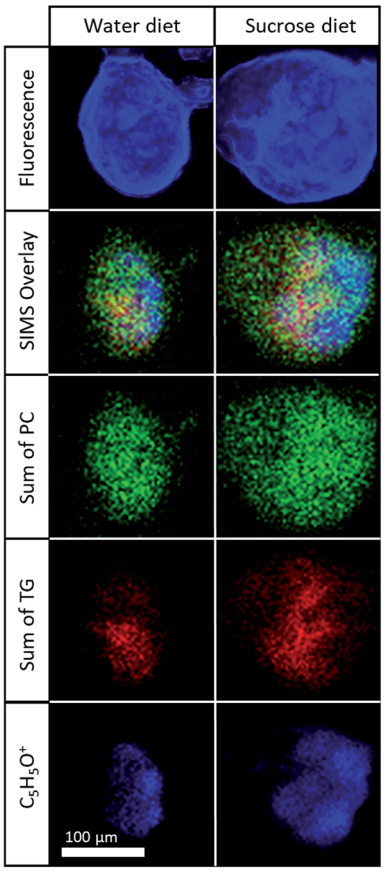

Fig. 4 Fluorescence and overlay of all 2D images from the 3D-MSI analysis (top view) of follicles from water- and sucrose-diet mosquitoes. DAPI staining allows fluorescence imaging of nurse cells. Secondary ion signal from selected *m*/*z* were used to visualize the distribution of phosphatidylcholine (PC), triacylglyceride (TG), and ribose within individual follicles. A typical SIMS spectrum is shown in Fig. S3.†

Polyunsaturated TG contents in ovarian follicles

All TGs identified contained either mono- or poly-unsaturated long-chain fatty acids (LCFA) with 16–20 carbons in each fatty acyl group (see Table 1). In Fig. 5, the secondary ion yield for thirteen selected TGs are compared for the two diet conditions. Ovarian follicles from sucrose-fed females exhibited increases in all the detected TGs, with differences between the two diets decreasing as the fatty acid chain length increased (greater differences in TG 48 and 50 *vs.* TG 52 and 54). These studies also revealed that the amounts of poly-unsaturated TGs, such as 50:4, 52:4 and 54:4, were less affected by the female diet. SIMS was also used to compare PCs in individual follicles from water-

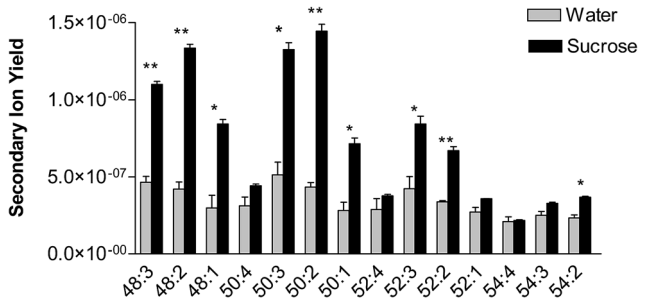

Fig. 5 Comparison of the sum triacylglyceride (TG) signal from the 3D-MSI analysis. The analysis was comprised of $n = 2$ individual follicles from a single water-fed, and a single sucrose-fed female. Bars represent the mean and the standard error of the mean (SEM) of duplicate measurements. Asterisks denote significant difference (unpaired t-test: $**p \leq 0.01$, $*p \leq 0.05$).

and sugar-fed females. There were not major differences in the signal of PCs from females raised with the two diets in the follicles sampled (ESI Fig. S2†). 3D-MSI trends in TG and PC relative abundances as a function of the diet agree with those from LC-MS/MS measurements. That is, TGs were found to be more abundant in extracts of sucrose-fed female ovaries while no major differences in the PCs between the two diets were observed (ESI Fig. S2†).

Triacylglycerides are the main lipid class stored in mosquito eggs as a long-term source of energy and nutrients.[72] Sugar-feeding resulted in a higher mobilization of saturated TG into the developing eggs. Previously, mosquito embryonic development has been demonstrated to be completed within ~3 days after oviposition, and fully developed 1st instar larvae reside for weeks/months within the chorion awaiting the appropriate environmental cues to stimulate hatching.[72] Reserves of TG with saturated fatty acids are very stable, whereas unsaturated acids are more susceptible to oxidation; the more double bonds, the greater the susceptibility. Mosquito pharate larvae can withstand months of quiescence inside the egg only depending on these stored "stable" maternal reserves.

Ovaries from mosquitoes reared under different nutritional conditions showed differences in follicle size, oocyte size, oocyte lipid contents, and overall morphology. Nutritional stress generated a more heterogeneous population of follicles with different intrinsic ''quality'', including dissimilar lipid reserves. These differences determine the potential of individual follicles for further development, and categorize them into "viable" and "unviable" follicles.[56] Unviable follicles have higher probability of being resorbed by apoptosis, this resorption of follicles represents a reversal of nutrients away from reproduction and towards alternative activities and reflects the need to balance present and future reproduction to maximize fitness.[55,56,73]

Conclusions

3D-TOF-SIMS analysis allowed for the recognition of different cell types within the mosquito ovarian follicle, as well as revealed changes of lipid species at the individual ovarian follicle level. A good agreement was observed between optical and 3D-TOF-SIMS derived structural features, differentiating the three main follicular components (oocyte, nurse cells, and follicular epithelial cells). Our studies revealed that stored polyunsaturated TGs increased in sucrose-fed insects; and therefore, these TG species could be used as markers for follicular fitness and overall mosquito reproductive output. Despite relative sample reproducibility per feeding condition, the current analysis consisted of $n = 2$ and more biological replicates will better support the trends observed. Further integration of this 3D-MSI probes with ultrahigh resolution instruments and tandem MS strategies will provide independent verification of the molecular composition at the single cell level and increase the analytical power of 3D-SIMS. The high homogeneity across the follicles (Fig. 1) between the two feeding conditions allows to more confidently extrapolate the 3D-TOF-SIMS results ($n = 2$ per feeding condition).

Conflicts of interest

The authors report that there are no conflicts of interest.

Acknowledgements

This work was supported by the NIH grant No. R21AI135469-01A1 to FFL. AC was fully supported by NRC Fellowship NRC-HQ-84-14-G-0040 as well as by NSF grant HRD-1547798. This material is based upon work supported by the National Science Foundation under Grant No. HRD-1547798. This NSF Grant was awarded to Florida International University as part of the Centers for Research Excellence in Science and Technology (CREST) Program. This is contribution number **900** from the Southeast Environmental Research Center in the Institute of Water & Environment at Florida International University. The authors thank Dan Graham, Ph.D., for developing the NESAC/BIO Toolbox used in this study and NIH grant EB-002027 for supporting the toolbox development.

References

1 T. Hu and J.-L. Zhang, Mass-spectrometry-based lipidomics, *J. Sep. Sci.*, 2017, **41**, 351–372.
2 Y. H. Rustam and G. E. Reid, Analytical Challenges and Recent Advances in Mass Spectrometry Based Lipidomics, *Anal. Chem.*, 2018, **90**, 374–397.
3 R. Bandu, H. J. Mok and K. P. Kim, Phospholipids as cancer biomarkers: Mass spectrometry-based analysis, *Mass Spectrom. Rev.*, 2016, **37**, 107–138.
4 C. Z. Ulmer, R. A. Yost, J. Chen, C. E. Mathews and T. J. Garrett, Liquid chromatography-mass spectrometry metabolic and lipidomic sample preparation workflow for suspension-cultured mammalian cells using Jurkat T lymphocyte cells, *J. Proteomics Bioinf.*, 2015, **8**, 360.
5 D. Veličković, R. K. Chu, A. A. Carrell, M. Thomas, L. Paša-Tolić, D. J. Weston and C. R. Anderton, Multimodal MSI in Conjunction with Broad Coverage Spatially Resolved MS2

Increases Confidence in Both Molecular Identification and Localization, *Anal. Chem.*, 2018, **90**, 702–707.
6 G. J. Van Berkel, V. Kertesz, K. A. Koeplinger, M. Vavrek and A.-N. T. Kong, Liquid microjunction surface sampling probe electrospray mass spectrometry for detection of drugs and metabolites in thin tissue sections, *J. Mass Spectrom.*, 2007, **43**, 500–508.
7 Z. Takáts, J. M. Wiseman, B. Gologan and R. G. Cooks, Mass Spectrometry Sampling Under Ambient Conditions with Desorption Electrospray Ionization, *Science*, 2004, **306**, 471.
8 R. G. Cooks, Z. Ouyang, Z. Takats and J. M. Wiseman, Ambient Mass Spectrometry, *Science*, 2006, **311**, 1566.
9 G. J. Van Berkel, A. D. Sanchez and J. M. E. Quirke, Thin-Layer Chromatography and Electrospray Mass Spectrometry Coupled Using a Surface Sampling Probe, *Anal. Chem.*, 2002, **74**, 6216–6223.
10 D. I. Campbell, C. R. Ferreira, L. S. Eberlin and R. G. Cooks, Improved spatial resolution in the imaging of biological tissue using desorption electrospray ionization, *Anal. Bioanal. Chem.*, 2012, **404**, 389–398.
11 L. Lamont, G. B. Eijkel, E. A. Jones, B. Flinders, S. R. Ellis, T. Porta Siegel, R. M. A. Heeren and R. J. Vreeken, Targeted Drug and Metabolite Imaging: Desorption Electrospray Ionization combined with Triple Quadrupole Mass Spectrometry, *Anal. Chem.*, 2018, **90**, 13229–13235.
12 R. Yin, J. Kyle, K. Burnum-Johnson, K. J. Bloodsworth, L. Sussel, C. Ansong and J. Laskin, High Spatial Resolution Imaging of Mouse Pancreatic Islets Using Nanospray Desorption Electrospray Ionization Mass Spectrometry, *Anal. Chem.*, 2018, **90**, 6548–6555.
13 A. Zavalin, J. Yang, K. Hayden, M. Vestal and R. M. Caprioli, Tissue protein imaging at 1 μm laser spot diameter for high spatial resolution and high imaging speed using transmission geometry MALDI TOF MS, *Anal. Bioanal. Chem.*, 2015, **407**, 2337–2342.
14 M. Karas and F. Hillenkamp, Laser desorption ionization of proteins with molecular masses exceeding 10,000 daltons, *Anal. Chem.*, 1988, **60**, 2299–2301.
15 R. M. Caprioli, T. B. Farmer and J. Gile, Molecular Imaging of Biological Samples: Localization of Peptides and Proteins Using MALDI-TOF MS, *Anal. Chem.*, 1997, **69**, 4751–4760.
16 T. C. Baker, J. Han and C. H. Borchers, Recent advancements in matrix-assisted laser desorption/ionization mass spectrometry imaging, *Curr. Opin. Biotechnol.*, 2017, **43**, 62–69.
17 E. Gemperline, S. Rawson and L. Li, Optimization and Comparison of Multiple MALDI Matrix Application Methods for Small Molecule Mass Spectrometric Imaging, *Anal. Chem.*, 2014, **86**, 10030–10035.
18 Q. P. Vanbellingen, A. Castellanos, M. Rodriguez-Silva, I. Paudel, J. W. Chambers and F. A. Fernandez-Lima, Analysis of Chemotherapeutic Drug Delivery at the Single Cell Level Using 3D-MSI-TOF-SIMS, *J. Am. Soc. Mass Spectrom.*, 2016, **27**, 2033–2040.
19 A. Henss, S.-K. Otto, K. Schaepe, L. Pauksch, K. S. Lips and M. Rohnke, High resolution imaging and 3D analysis of Ag nanoparticles in cells with ToF-SIMS and delayed extraction, *Biointerphases*, 2018, **13**, 03B410.
20 S. Sämfors, M. Ståhlman, M. Klevstig, J. Borén and J. S. Fletcher, Localised lipid accumulation detected in infarcted mouse heart tissue using ToF-SIMS, *Int. J. Mass Spectrom.*, 2019, **437**, 77–86.
21 H. Tian, L. J. Sparvero, A. A. Amoscato, A. Bloom, H. Bayır, V. E. Kagan and N. Winograd, Gas Cluster Ion Beam Time-of-Flight Secondary Ion Mass Spectrometry High-Resolution Imaging of Cardiolipin Speciation in the Brain: Identification of Molecular Losses after Traumatic Injury, *Anal. Chem.*, 2017, **89**, 4611–4619.
22 S. Chandra, W. A. Ausserer and G. H. Morrison, Evaluation of matrix effects in ion microscopic analysis of freeze-fractured, freeze-dried cultured cells, *J. Microsc.*, 1987, **148**, 223–229.
23 G. Slodzian, Étude d'une méthode d'analyse locale chimique et isotopique utilisant l'émission ionique secondaire, *Ann. Phys.*, 1964, **13**, 591–648.
24 A. Brunelle, D. Touboul and O. Laprevote, Biological tissue imaging with time-of-flight secondary ion mass spectrometry and cluster ion sources, *J. Mass Spectrom.*, 2005, **40**, 985.
25 D. Touboul, F. Halgand, A. Brunelle, R. Kersting, E. Tallarek, B. Hagenhoff and O. Laprévote, Tissue Molecular Ion Imaging by Gold Cluster Ion Bombardment, *Anal. Chem.*, 2004, **76**, 1550–1559.
26 M. P. Seah, R. Havelund and I. S. Gilmore, Universal Equation for Argon Cluster Size-Dependence of Secondary Ion Spectra in SIMS of Organic Materials, *J. Phys. Chem. C*, 2014, **118**, 12862–12872.
27 E. Niehuis, R. Möllers, D. Rading, H. G. Cramer and R. Kersting, Analysis of organic multilayers and 3D structures using Ar cluster ions, *Surf. Interface Anal.*, 2013, **45**, 158–162.
28 M. P. Seah, Universal Equation for Argon Gas Cluster Sputtering Yields, *J. Phys. Chem. C*, 2013, **117**, 12622–12632.
29 F. A. Fernandez-Lima, J. Post, J. D. DeBord, M. J. Eller, S. V. Verkhoturov, S. Della-Negra, A. S. Woods and E. A. Schweikert, Analysis of Native Biological Surfaces Using a 100 kV Massive Gold Cluster Source, *Anal. Chem.*, 2011, **83**, 8448–8453.
30 K. J. Adams, J. D. DeBord and F. Fernandez-Lima, Lipid specific molecular ion emission as a function of the primary ion characteristics in TOF-SIMS, *J. Vac. Sci. Technol., B: Nanotechnol. Microelectron.: Mater., Process., Meas., Phenom.*, 2016, **34**, 051804.
31 M. G. Blain, S. Della-Negra, H. Joret, Y. Le Beyec and E. A. Schweikert, Secondary-ion yields from surfaces bombarded with keV molecular and cluster ions, *Phys. Rev. Lett.*, 1989, **63**, 1625.
32 R. D. Harris, N. J. Vanstipdonk and E. A. Schweikert, keV Cluster Impacts: Prospects for Cluster-SIMS, *Int. J. Mass Spectrom. Ion Processes*, 1998, **174**, 167–177.
33 S. Della-Negra, J. Depauw, C. Guillermier and E. A. Schweikert, Massive clusters: Secondary emission from qkeV to qMeV. New emission processes? New SIMS probe?, *Surf. Interface Anal.*, 2011, **43**, 62–65.

34 J. S. Fletcher, N. P. Lockyer, S. Vaidyanathan and J. C. Vickerman, TOF-SIMS 3D Biomolecular Imaging of Xenopus laevis Oocytes Using Buckminsterfullerene (C60) Primary Ions, *Anal. Chem.*, 2007, **79**, 2199–2206.
35 D. Weibel, S. Wong, N. Lockyer, P. Blenkinsopp, R. Hill and J. C. Vickerman, A C60 Primary Ion Beam System for Time of Flight Secondary Ion Mass Spectrometry: Its Development and Secondary Ion Yield Characteristics, *Anal. Chem.*, 2003, **75**, 1754–1764.
36 M. J. van Stipdonk, R. D. Harris and E. A. Schweikert, A Comparison of Desorption Yields from C+60 to Atomic and Polyatomic Projectiles at keV Energies, *Rapid Commun. Mass Spectrom.*, 1996, **10**, 1987–1991.
37 S. Ninomiya, K. Ichiki, H. Yamada, Y. Nakata, T. Seki, T. Aoki and J. Matsuo, Molecular depth profiling of multilayer structures of organic semiconductor materials by secondary ion mass spectrometry with large argon cluster ion beams, *Rapid Commun. Mass Spectrom.*, 2009, **23**, 3264–3268.
38 K. Moritani, M. Hashinokuchi, J. Nakagawa, T. Kashiwagi, N. Toyoda and K. Mochiji, Extremely low-energy projectiles for SIMS using size-selected gas cluster ions, *Appl. Surf. Sci.*, 2008, **255**, 948–950.
39 S. Sheraz née Rabbani, A. Barber, J. S. Fletcher, N. P. Lockyer and J. C. Vickerman, Enhancing secondary ion yields in time of flight-secondary ion mass spectrometry using water cluster primary beams, *Anal. Chem.*, 2013, **85**, 5654–5658.
40 H. Tian, D. Maciążek, Z. Postawa, B. J. Garrison and N. Winograd, CO_2 Cluster Ion Beam, an Alternative Projectile for Secondary Ion Mass Spectrometry, *J. Am. Soc. Mass Spectrom.*, 2016, **27**, 1476–1482.
41 C. Bich, R. Havelund, R. Moellers, D. Touboul, F. Kollmer, E. Niehuis, I. S. Gilmore and A. Brunelle, Argon Cluster Ion Source Evaluation on Lipid Standards and Rat Brain Tissue Samples, *Anal. Chem.*, 2013, **85**, 7745.
42 S. M. Khalil, A. Roempp, J. Pretzel, K. Becker and B. Spengler, Phospholipid Topography of Whole-Body Sections of the Anopheles stephensi Mosquito, Characterized by High-Resolution Atmospheric-Pressure Scanning Microprobe Matrix-Assisted Laser Desorption/Ionization Mass Spectrometry Imaging, *Anal. Chem.*, 2015, **87**, 11309–11316.
43 T. N. Phan Nhu, S. Fletcher John, P. Sjövall and G. Ewing Andrew, ToF-SIMS imaging of lipids and lipid related compounds in Drosophila brain, *Surf. Interface Anal.*, 2014, **46**, 123–126.
44 D. Bhandari, M. Schott, A. Römpp, A. Vilcinskas and B. Spengler, Metabolite localization by atmospheric pressure high-resolution scanning microprobe matrix-assisted laser desorption/ionization mass spectrometry imaging in whole-body sections and individual organs of the rove beetle *Paederus riparius*, *Anal. Bioanal. Chem.*, 2015, **407**, 2189–2201.
45 F. Kaftan, V. Vrkoslav, P. Kynast, P. Kulkarni, S. Böcker, J. Cvačka, M. Knaden and A. Svatoš, Mass spectrometry imaging of surface lipids on intact Drosophila melanogaster flies, *J. Mass Spectrom.*, 2014, **49**, 223–232.
46 G. Zhou, J. E. Pennington and M. A. Wells, Utilization of pre-existing energy stores of female Aedes aegypti mosquitoes during the first gonotrophic cycle, *Insect Biochem. Mol. Biol.*, 2004, **34**, 919–925.
47 H. Briegel, I. Knusel and S. E. Timmermann, Aedes aegypti: size, reserves, survival, and flight potential, *J. Vector Ecol.*, 2001, **26**, 21–31.
48 H. H. Hagedorn, The Control of Vitellogenesis in the Mosquito, Aedes aegypti, *Am. Zool.*, 1974, **14**, 1207–1217.
49 S. Bhatt, P. W. Gething, O. J. Brady, J. P. Messina, A. W. Farlow, C. L. Moyes, J. M. Drake, J. S. Brownstein, A. G. Hoen, O. Sankoh, M. F. Myers, D. B. George, T. Jaenisch, G. R. W. Wint, C. P. Simmons, T. W. Scott, J. J. Farrar and S. I. Hay, The global distribution and burden of dengue, *Nature*, 2013, **496**, 504.
50 S. C. Weaver and W. K. Reisen, Present and future arboviral threats, *Antiviral Res.*, 2010, **85**, 328–345.
51 D. Musso and D. J. Gubler, Zika Virus, *Clin. Microbiol. Rev.*, 2016, **29**, 487.
52 R. G. A. Feachem, A. A. Phillips, J. Hwang, C. Cotter, B. Wielgosz, B. M. Greenwood, O. Sabot, M. H. Rodriguez, R. R. Abeyasinghe, T. A. Ghebreyesus and R. W. Snow, Shrinking the malaria map: progress and prospects, *Lancet*, 2010, **376**, 1566–1578.
53 A. N. Clements, *The biology of mosquitoes. Development, nutrition and reproduction*, CABI Publishing, New York, NY, 1992.
54 M. J. Klowden, Endocrine aspects of mosquito reproduction, *Arch. Insect Biochem. Physiol.*, 1997, **35**, 491–512.
55 M. E. Clifton and F. G. Noriega, Nutrient limitation results in juvenile hormone-mediated resorption of previtellogenic ovarian follicles in mosquitoes, *J. Insect Physiol.*, 2011, **57**, 1274–1281.
56 M. E. Clifton and F. G. Noriega, The fate of follicles after a blood meal is dependent on previtellogenic nutrition and juvenile hormone in Aedes aegypti, *J. Insect Physiol.*, 2012, **58**, 1007–1019.
57 R. Ziegler and M. M. Ibrahim, Formation of lipid reserves in fat body and eggs of the yellow fever mosquito, Aedes aegypti, *J. Insect Physiol.*, 2001, **47**, 623–627.
58 E. Van Handel, The obese mosquito, *J. Physiol.*, 1965, **181**, 478–486.
59 S. Chandra, G. H. Morrison and C. C. Wolcott, Imaging intracellular elemental distribution and ion fluxes in cultured cells using ion microscopy: a freeze-fracture methodology, *J. Microsc.*, 1986, **144**, 15–37.
60 E. S. F. Berman, S. L. Fortson, K. D. Checchi, L. Wu, J. S. Felton, K. J. J. Wu and K. S. Kulp, Preparation of single cells for imaging/profiling mass spectrometry, *J. Am. Soc. Mass Spectrom.*, 2008, **19**, 1230–1236.
61 J. Malm, D. Giannaras, M. O. Riehle, N. Gadegaard and P. Sjövall, Fixation and Drying Protocols for the Preparation of Cell Samples for Time-of-Flight Secondary Ion Mass Spectrometry Analysis, *Anal. Chem.*, 2009, **81**, 7197–7205.
62 J. S. Fletcher, S. Rabbani, A. Henderson, N. P. Lockyer and J. C. Vickerman, Three-dimensional mass spectral imaging

of HeLa-M cells – sample preparation, data interpretation and visualisation, *Rapid Commun. Mass Spectrom.*, 2011, **25**, 925–932.
63 G. C. Atella, K. C. Gondim, E. A. Machado, M. N. Medeiros, M. A. C. Silva-Neto and H. Masuda, Oogenesis and egg development in triatomines: a biochemical approach, *An. Acad. Bras. Cienc.*, 2005, **77**, 405–430.
64 E. Van Handel, Fuel metabolism of the mosquito (Culex quinquefasciatus) embryo, *J. Insect Physiol.*, 1993, **39**, 831–833.
65 H. Briegel, M. Hefti and E. DiMarco, Lipid metabolism during sequential gonotrophic cycles in large and small female Aedes aegypti, *J. Insect Physiol.*, 2002, **48**, 547–554.
66 J. D. DeBord, D. F. Smith, C. R. Anderton, R. M. Heeren, L. Pasa-Tolic, R. H. Gomer and F. A. Fernandez-Lima, Secondary Ion Mass Spectrometry Imaging of Dictyostelium discoideum Aggregation Streams, *PLoS One*, 2014, **9**, e99319.
67 S. Chandra, 3D subcellular SIMS imaging in cryogenically prepared single cells, *Appl. Surf. Sci.*, 2004, **231–232**, 467–469.
68 M. A. Robinson, D. J. Graham and D. G. Castner, ToF-SIMS Depth Profiling of Cells: z-Correction, 3D Imaging, and Sputter Rate of Individual NIH/3T3 Fibroblasts, *Anal. Chem.*, 2012, **84**, 4880–4885.
69 C. F. Newman, R. Havelund, M. K. Passarelli, P. S. Marshall, I. Francis, A. West, M. R. Alexander, I. S. Gilmore and C. T. Dollery, Intracellular Drug Uptake—A Comparison of Single Cell Measurements Using ToF-SIMS Imaging and Quantification from Cell Populations with LC/MS/MS, *Anal. Chem.*, 2017, **89**, 11944–11953.
70 A. N. Rao, N. Vandencasteele, L. J. Gamble and D. W. Grainger, High resolution epifluorescence and TOF-SIMS chemical imaging comparisons of single DNA microarray spots, *Anal. Chem.*, 2012, **84**, 10628–10636.
71 C. J. May, H. E. Canavan and D. G. Castner, Quantitative X-ray Photoelectron Spectroscopy and Time-of-Flight Secondary Ion Mass Spectrometry Characterization of the Components in DNA, *Anal. Chem.*, 2004, **76**, 1114–1122.
72 M. H. Perez and F. G. Noriega, *Aedes aegypti* pharate 1st instar quiescence affects larval fitness and metal tolerance, *J. Insect Physiol.*, 2012, **58**, 824–829.
73 C. L. Boggs and C. L. Ross, The Effect of Adult Food Limitation on Life History Traits in *Speyeria Mormonia* (Lepidoptera: Nymphalidae), *Ecology*, 1993, **74**, 433–441.